Natural Frequency Analysis and Optimization Design of Rectangular Thin Plates With Nonlinear Variable-Thickness

Quanmin Xie

The State Key Laboratory of Fine Blasting, Jianghan University, Wuhan 430056, China.
Hubei Key Laboratory of Blasting Engineering, Jianghan University, Wuhan 430056, China.

Fengxiang Xu, Zhen Zou, Xiaoqiang Niu and Zhuang Dong

Hubei Key Laboratory of Advanced Technology of Automotive Components, Wuhan University of Technology, Wuhan 430070, China.
Hubei Collaborative Innovation Center for Automotive Components Technology, Wuhan University of Technology, Wuhan 430070, China. E-mail: xufx@whut.edu.cn

(Received 25 April 2022; accepted 28 July 2022)

Variable-thickness thin plate structures have been widely employed in many engineering applications, such as the automotive industry, aviation industry and civil structures. In this paper, natural frequency and optimization design of nonlinear variable-thickness rectangular thin plates are performed. For this purpose, theoretical solutions of dimensionless natural frequency of the bidirectional linear variable-thickness thin plates are conducted on the three classical boundaries to verify the correctness of a conducted numerical model. Then the natural frequencies of variable thickness plates with different forms including bidirectional and unidirectional nonlinear were compared. Additionally, the difference in vibration characteristics between the thin plate of variable thickness and the corresponding thin plate of equal mass are compared and analyzed, and the results show that when the middle part of the thin plate is thick, the natural frequency increases by a greater percentage. Finally, a new bidirectional stepped variable-thickness plate is proposed to improve the natural frequency of variable-thickness thin plates. Inspired by the stepped idea, the square and circle division methods are employed to improve the natural frequency of variable thickness thin plates, as the optimal design is carried out. The results show that the nonlinear variable thickness after performing an optimal design could significantly improve the natural frequency of thin plates. The finding provides useful insight into the structural design of variable thickness plates for free vibration.

1. INTRODUCTION

A variable-thickness thin plate structure, as one typical type of structure, has been widely employed in many engineering applications, such as the automotive industry, aviation industry and civil structures, due to their desirable mechanical properties such as outstanding lightweight and high strength.[1–4] Therefore, examining the vibrational behaviors of plates with a wide variety gains importance. Hence, many studies have been presented to examine the mechanical behaviors of various kinds of plates using different analytical and numerical approaches.[5–9] However, the vibration control equation of a rectangular plate with variable thicknesses is a fourth-order partial differential equation (PDE) with variable coefficients, therefore the analytical solution of the natural frequency can only be obtained in rare cases.[10,11]

In order to understand the vibration characteristics of thin plates with variable thickness, various numerical methods have been conducted, such as the finite difference method, finite element method, finite slat method, differential Quadrature method, mesh-less method, Green function method etc.[12–22] For instance, Malekzadeh and Singh verified the natural frequency of the variable thickness thin plate by using the differential quadrature scheme to solve the variable-thickness thin plates under the classical boundary.[23,24] Li et al. proposed an analytical method that can directly obtain all the series expansions for up to the fourth-order derivatives through term-by-term differentiation of the displacement series.[25–27] Ye et al. developed a modified Fourier solution based on the first-order shear deformation theory for the free vibration problems of moderately thick composite laminated plates with general boundary restraints and internal line supports.[28] Yuan and Chen proposed a novel analytical method to reduce such governing equations for circular plates to a pair of uncoupled and easily solvable differential equations of the Sturm-Liouville type.[29] According to these previous studies, it can be found that the theoretical research on the problem of plate vibration has been sufficiently studied.

Moreover, mechanical properties of the variable thickness plate have been widely studied for its advantage of reducing the weight of the structure as much as possible while ensuring the strength of the structure. Xu and Zhou studied the stress and displacement distributions of rectangular plates with continuously and functionally graded varying thicknesses that are simply supported at four edges.[30,31] Vivio and Vullo presented a new analytical method for the evaluation of elastic stresses and deformations in axisymmetric plates having variable thickness.[32] Dozio presented a new variable kinematic Ritz method applied to free vibration analysis of arbitrary quadrilateral thin and thick isotropic plates.[33] Semnani et al. extended the application of the two-dimensional differential transform method to study the free vibration of thin plates with an arbitrarily varying thickness.[34] Thai et al. presented a new inverse tangent shear deformation theory (ITSDT) for the static, free vibration and buckling analysis of laminated composite and sandwich plates.[35] Mashat analyzed hygrothermal bending response of the sector-shaped annular plate with variable radial thickness based on Kirchhoff plate theory.[36] Zenkour developed the exact analytical solutions for the bending behavior of thin rectangular plates subjected to a transverse uniformly distributed load.[37] From the above literature, it can be seen that many researchers of the vibration characteristics of Variable-thickness Rolled Blanks (VRB) have mostly concentrated on calculating the vibration characteristics of VRB under different elastic boundary conditions and distribution forms using various solution methods. However, they have not paid attention to the differences in vibration characteristics between the VRB of the same mass and Equal-thickness Rolled Blanks (ERB), and there is less research on the optimization techniques for thickness distribution of VRB.

With the rapid development of computer-aided design theory and the wide application in the field of engineering design and manufacturing, multi-objective optimization techniques have been applied in the design of various thin plates and have achieved many achievements. For instance, according to a given number of linear segments and plate volume, Chou et al. obtained the optimal thickness parameters and segment lengths through iterative optimization procedures and the Ritz method, and finally optimized the vibration problem of the circular Mindlin thin plate, maximizing the fundamental frequency of its free vibration.[38] Belblidia studied fully integrated design optimization (FIDO) of plate structures.[39] Dong-Kwon Kim optimized the thermal performance of a vertical plate-fin heat sink under natural convection for the case in which the fin thickness varied in the direction normal to the fluid flow.[40] Lee presented optimizing structural topology patterns using regularization of Heaviside function.[41] Banh proposed a compliance multi-material topology optimization design of continuum structures with the dependence of crack patterns.[42] Banh also presented a multi-material topology optimization approach for thin plates with variable thickness based on the Kirchhoff plate theory.[43] The above mentioned research studies have proved that the multi-objective optimization technique is one of the effective ways to rapidly improve the vibration characteristics of thin plates.

In this paper, taking the rectangular thin plate as a point, the difference in natural frequency and vibration characteristics between the thin plates with variable thickness and with equal thickness was studied and compared. Then, the change law and characteristics of the vibration thickness of thin plates in different forms were summarized. Additionally, according to the previous step's law, the thickness distribution form was optimized to obtain an optimally distributed variable thickness thin plate structure. In the end, under the premise of a certain mass, the first-order natural frequency of the thin plate is maximized, the structure is optimized, and the weight is lightened.

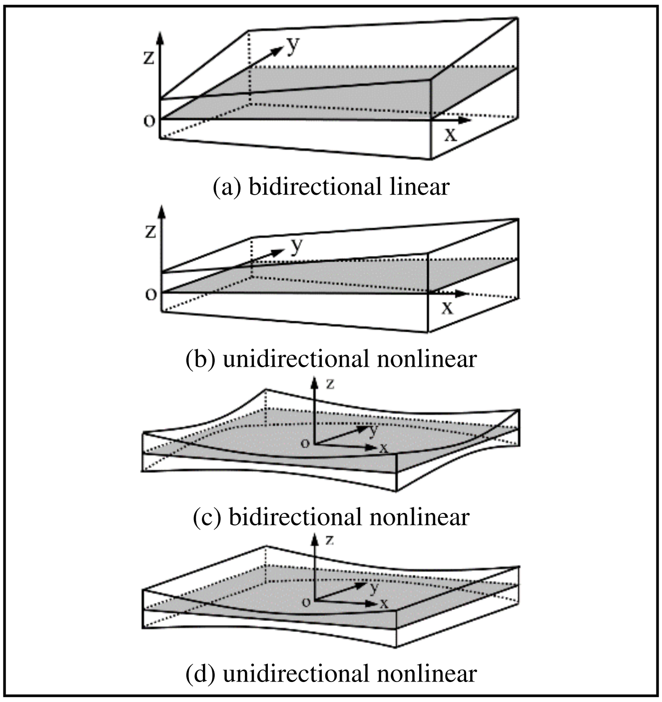

Figure 1. Schematic diagram of linear and nonlinear variable thickness thin plate.

2. THEORETICAL MODEL AND VERIFICATION

Variable-thickness thin plates can be divided into two types according to the changing trend of the variable-thickness plate: bidirectional linear variable-thickness thin plates and bidirectional nonlinear variable-thickness thin plates. Especially, when the change rate of a bidirectional linear/non-linear variable-thickness plate in one direction is 0, it becomes a unidirectional linear/non-linear variable-thickness plate, as shown in Fig. 1. Therefore, in this paper, only bidirectional linear variable thickness thin plates and bidirectional nonlinear variable thickness thin plates are modeled and verified.

To validate the accuracy of the numerical models of variable-thickness thin plates, in this section, theoretical solutions and numerical solutions that were obtained by the commercial software package ABAQUS were obtained on the three classical boundaries which are free (FNo restrictions), simply supported (S U1=U2=U3=0) and fixed (C U1=U2=U3=UR1=UR2=UR3=0).

2.1. Comparisons and Numerical Results

The comparison between theoretical predictions and FE simulations of the dimensionless natural frequency Ω_1 of the bidirectional linear variable-thickness thin plate is shown in Table 1. The theoretical predictions of the dimensionless natural frequency were obtained from the reference.[8] The comparison between theoretical predictions and FE simulations for the dimensionless natural frequency Ω_2 of the bidirectional nonlinear variable-thickness thin plate is shown in Table 2.

From Table 1 and Table 2, it can be observed that the difference between theoretical predictions and FE simulations is within 1%, which shows that the FE modeling is accurate and feasible.

Table 1. Comparison of dimensionless natural frequency Ω_1 and theoretical solution ($\Omega_1 = \omega a\sqrt{\rho h/D}$).

BC	α	-0.5		-0.5		0.5	
	β	-0.5		0.5		0.5	
	order	FEM	Ref[8]	FEM	Ref[8]	FEM	Ref[8]
CCCF	1	19.211	19.209	32.562	32.565	55.176	55.208
	2	38.343	38.327	65.446	65.439	111.640	111.720
	3	39.249	39.238	66.483	66.480	112.570	112.660
SSSS	1	10.801	10.812	18.139	18.173	30.448	30.553
	2	25.918	25.970	44.169	44.245	75.100	75.300
	3	26.823	26.832	45.135	45.183	76.029	76.211
CCCF	1	11.214	11.225	23.587	23.624	39.969	40.061
	2	21.635	21.651	36.595	36.652	61.876	62.042
	3	28.110	28.142	61.662	61.739	104.520	104.710
SSSF	1	6.117	6.124	11.137	11.148	18.856	18.887
	2	15.323	15.353	25.531	25.593	42.811	42.996
	3	19.300	19.336	40.073	40.120	67.686	67.801

Table 2. Comparison of dimensionless natural frequency Ω_2 and theoretical solution ($\Omega_2 = \omega a^2\sqrt{\rho h/D}$).

Order	Classic boundary conditions					
	FFFF		SSSS		CCCC	
	FEM	Ref[9]	FEM	Ref[9]	FEM	Ref[9]
1	21.875	21.949	34.388	34.649	61.433	61.476
2	32.730	32.763	79.582	79.916	119.270	119.390
3	38.997	39.026	82.671	82.967	122.290	122.420
4	57.686	57.913	133.510	134.230	182.610	182.960
5	58.506	58.667	155.510	155.850	208.450	208.720
6	91.458	91.635	156.130	156.470	209.810	210.080

Table 3. Thickness distribution of variable-thickness thin plates.

Types of plates	Thickness change equation	parameters
Unidirectional linear	$h = h_0\left(1+\alpha\frac{x}{a}\right)$	α
Bidirectional linear	$h = h_0\left(1+\alpha\frac{x}{a}\right)\left(1+\beta\frac{y}{b}\right)$	α, β
Unidirectional nonlinear	$h_1 = h_0\left[1+\alpha\left(\frac{x}{a/2}\right)^m\right]$ $h_2 = h_0\left[6-\alpha\left(\frac{x}{a/2}\right)^m\right]$	α, m
Bidirectional nonlinear	$h_1 = h_0\left[1+\alpha\left(\frac{x}{a/2}\right)^m\right]\left[1+\beta\left(\frac{x}{b/2}\right)^n\right]$ $h_2 = h_0\left[6-\alpha\left(\frac{x}{a/2}\right)^m\right]\left[6-\beta\left(\frac{x}{b/2}\right)^n\right]$	α, β, m, n

3. VIBRATION CHARACTERISTICS OF VARIABLE-THICKNESS THIN PLATES

3.1. Changing Forms of Variable Thickness

The thickness distribution has a great influence on the vibration characteristics of variable-thickness thin plates; hence it is necessary to study the vibration characteristics of variable-thickness thin plates under classical boundary conditions. Four different thickness distribution forms are shown in Table 3. In order to ensure the comparability of the data, the size and material properties of the thin plate are identical ($a = b = 0.5$ m, $h_0 = 0.001$ m, $E = 210$ GPa, $\rho = 7800$ kg/m^3, $\mu = 0.3$).

In order to conform to the thin plate vibration theory, above-mentioned change parameters are respectively taken as: unidirectional linearity $\alpha = 1/2/3/4/5$; bidirectional linearity $\alpha = \beta = 0.5/1/1.5/2/2.5$; unidirectional nonlinearity $\alpha = 1/2/3/4/5$, $m = 2/4/6/8/10$; and bidirectional nonlinearity $\alpha = \beta = 0.5/1/1.5/2/2.5$, $m = n = 2/4/6/8/10$. Different variable-thickness thin plate diagrams are shown in Fig. 2, 3, and 4. The left side is schematic diagrams of the thin plate, and the right side is the cloud map.

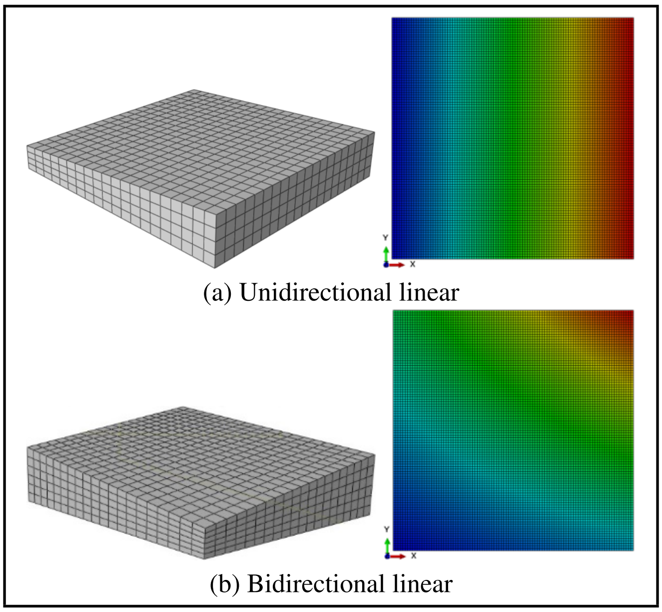

(a) Unidirectional linear

(b) Bidirectional linear

Figure 2. Linear variable thickness plate.

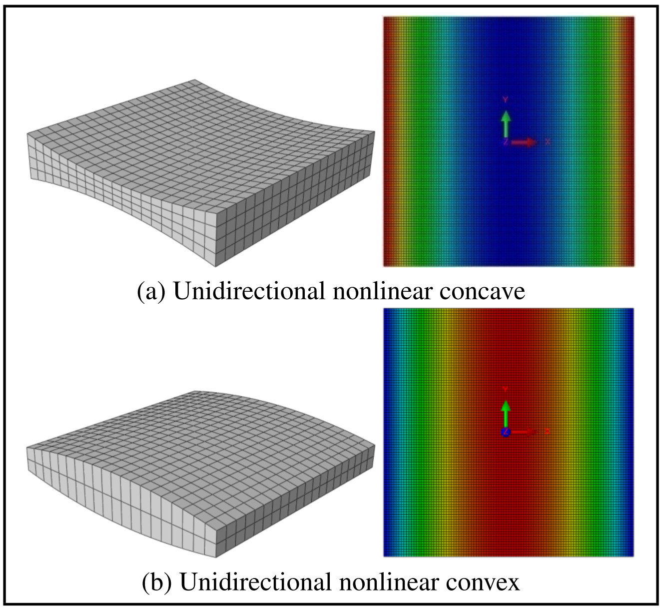

(a) Unidirectional nonlinear concave

(b) Unidirectional nonlinear convex

Figure 3. Unidirectional nonlinear variable thickness thin plate.

The center point of unidirectional non-linear variable-thickness thin plates that include unidirectional non-linear concave variable-thickness thin plates and unidirectional nonlinear convex variable-thickness thin plates are selected as the origin of the coordinate system due to its symmetry, which is shown in Fig. 3.

The mass m is controlled unchanged, and ERB of the same size are established, meanwhile, other parameters are ensured consistent, namely:

$$M_{VRB} = M_{ERB}; \tag{1}$$

$$h_D = \frac{M_ERB}{ab}; \tag{2}$$

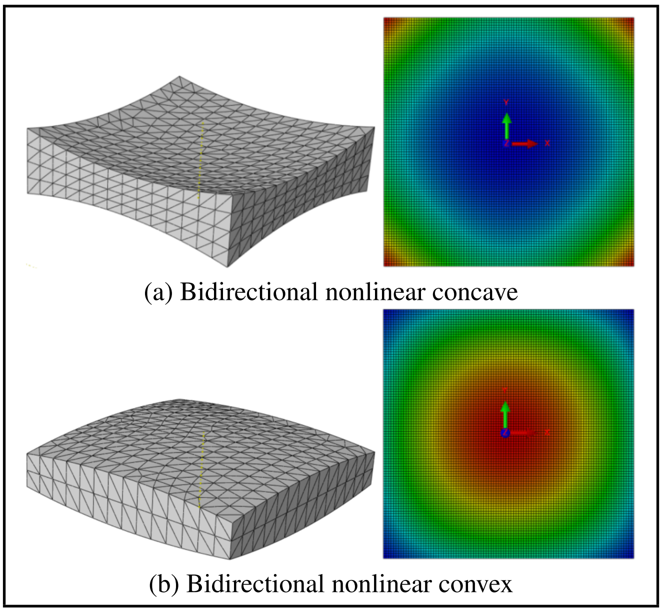

(a) Bidirectional nonlinear concave

(b) Bidirectional nonlinear convex

Figure 4. Bidirectional nonlinear variable thickness thin plate.

where M_{VRB} is the mass of the variable-thickness plate, M_{ERB} is the mass of the equal-thickness plate and h_D is the equivalent thickness.

3.2. Comparison of Natural Frequencies of Different Forms

In order to express the increase or decrease of the natural frequency of the variable-thickness sheet, defining the parameter A, which takes the difference between the natural frequency of the variable-thickness thin plate and the equal-thickness plate as the numerator, and takes the natural frequency of the equal-thickness plate as the denominator:

$$A = \frac{f_{VRB} - f_{ERB}}{f_{ERB}} \times 100\%. \tag{3}$$

Figure 5 is a graph of percentage A when variable-thickness thin plate type is unidirectional linear ($\alpha = 1/2/3/4/5$). Five kinds of unidirectional linear variable-thickness thin plates are established separately, and their free vibration characteristics can be obtained under simply supported and fixed supported boundary conditions. Obtaining the corresponding equivalent thickness according to Eq. (2), analyzing the vibration characteristics of the thin plate with the same thickness under the same conditions, and finally finding the change curve between the percentage A and the changing parameter will be employed. Similarly, other variable-thickness sheets' changing graphs of the percentage A can be obtained, as shown in Fig. 6, 7, 8, 9 and 10. Regarding graphs (a), (b) and (c), each figure corresponds to the natural frequency percentage change of the changing parameters under three classical boundary conditions of free boundary conditions respectively. Graph (d) is a changing graph of the first-order natural frequency percentage of each type of thin plate as the change parameter increases under three classical boundary conditions.

Based on the above analysis for the first-order natural frequency, it is found that the growth rate of natural frequency on the free boundary conditions is not obvious (only 1–2 Hz) when the thickness of the thin plate changes linearly in one or two directions. On the contrary, the natural frequency will decline on a simple support and a fixed support. The percentage of natural frequency will decline when the thin plate thickness changes its form to concave on the free boundary, and the natural frequency will rise on the simple and fixed-supported boundary. However, when the thin plate thickness changes its form to convex, all things are the opposite.

From the previous research results, it can be seen that the unidirectional and bidirectional linear variable-thickness thin plates are basically not conducive to increasing the natural frequency Therefore, the other four variable thickness thin plates are considered comprehensively (unidirectional concave, unidirectional convex, bidirectional concave and bidirectional convex).

As shown in Fig. 11, the first three natural frequency increase percentage A under the classical boundary conditions. Bidirectional and unidirectional convex VRB can significantly increase the natural frequency on the FFFF boundary conditions, but the change is not obvious on the SSSS and CCCC boundary conditions. Meanwhile, the percentage change of bidirectional convex VRB is higher than unidirectional convex VRB. Obviously, when the thickness is concentrated in the middle of the thin plate, the natural frequency will increase effectively on the boundary condition of FFFF. The natural frequencies of the unidirectional and bidirectional concave VRB on the FFFF boundary condition will decline significantly, however first-order natural frequency will slightly increase on the SSSS and CCCC boundary conditions. It can be seen that when the thickness is scattered around the thin plate, the natural frequency on the FFFF boundary conditions will decline.

4. OPTIMIZATION DESIGN OF VARIABLE THICKNESS THIN PLATE

One of the effective approaches to improving the natural frequency of thin plates is by optimization. However, most research currently is to optimize the thickness of the whole thin plate, and there are few studies on continuous variable thickness optimization for individual thin plates, which makes it difficult to maximize the natural frequency of thin plates. In order to elevate the natural frequencies of thin plates, a new bidirectional stepped variable-thickness thin plate is proposed that possesses a new thickness distribution form: thick in the middle and edges. As shown in Fig. 14, Fig. 14 (a) is a bidirectional schematic diagram of the stepped VRB, and Fig. 14 (b) is the cloud map.

4.1. A New Bidirectional Stepped VRB

In order to elevate the natural frequencies of thin plates, a new bidirectional stepped variable-thickness thin plate is proposed that possesses a new thickness distribution form: thick in the middle and edges. As shown in Fig. 12, Fig. 12 (a) is bidirectional schematic diagram of the stepped VRB, and Fig. 14 (b) is the cloud map.

The bidirectional stepped VRB is affected by middle step width L and the step thickness t. $L = 0.15$ m and $t = 1.2/1.4/1.6/1.8/2.0$ mm are selected as an example. The thickness of other parts of the thin plate is set as 1 mm, and the length and width are set as 0.5 m. Meanwhile, the material properties are consistent with the above-mentioned figures. As

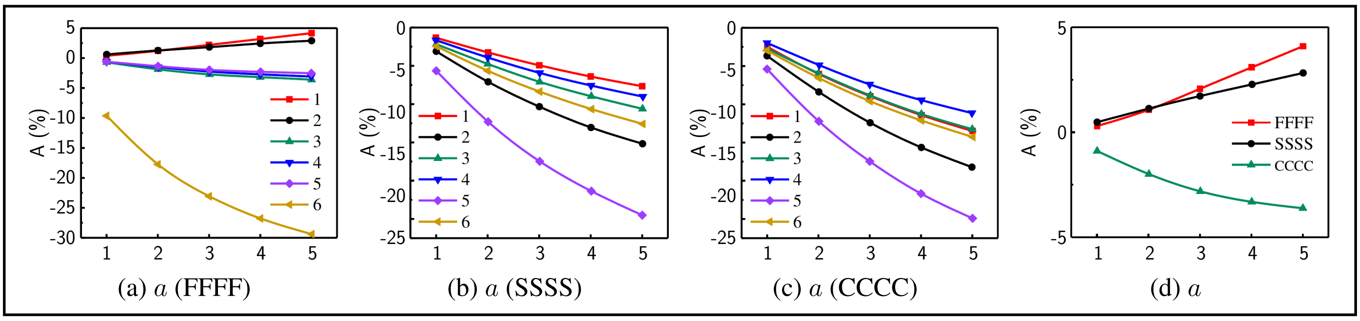

Figure 5. Percent change graph of natural frequency of unidirectional linear variable thickness plate.

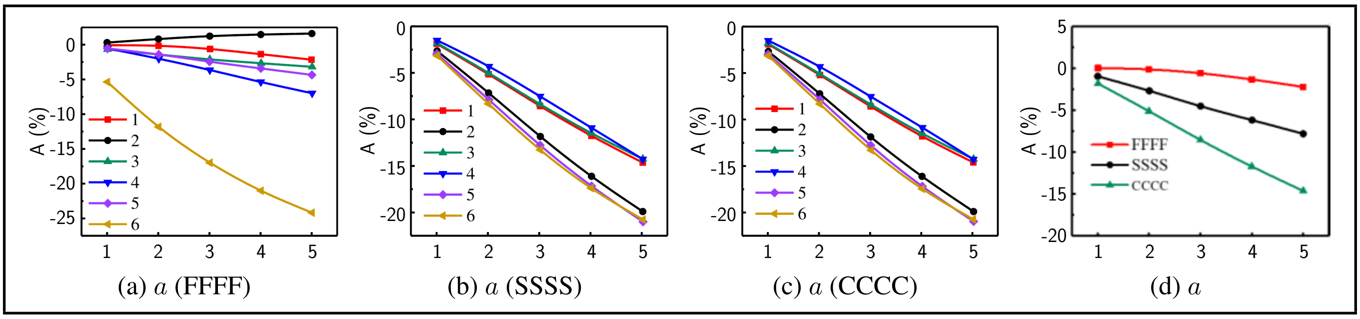

Figure 6. Percent change graph of natural frequency of bidirectional linear variable thickness plate.

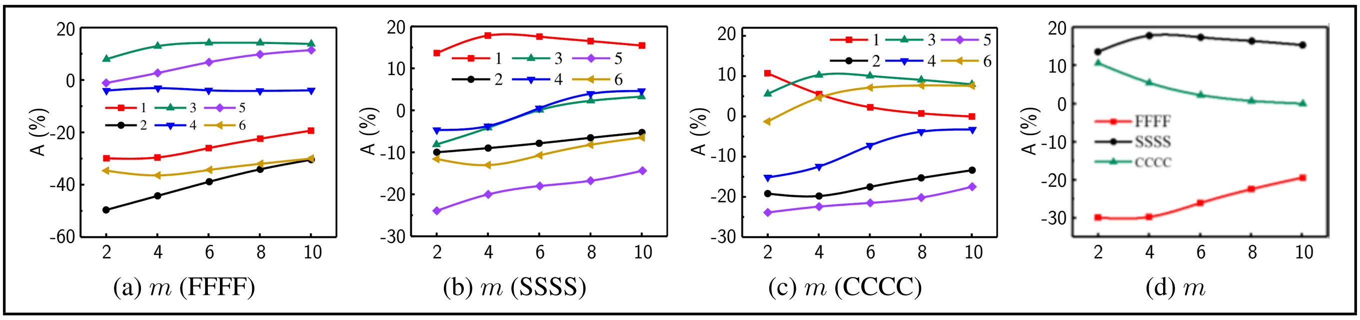

Figure 7. Percent change graph of natural frequency of unidirectional nonlinear concave thickness plate.

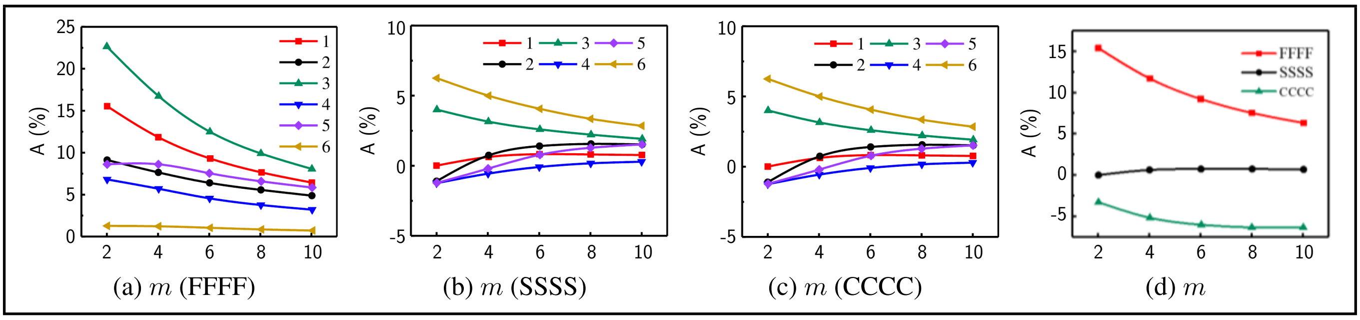

Figure 8. Percentage change of natural frequency of unidirectional nonlinear variable thickness plate.

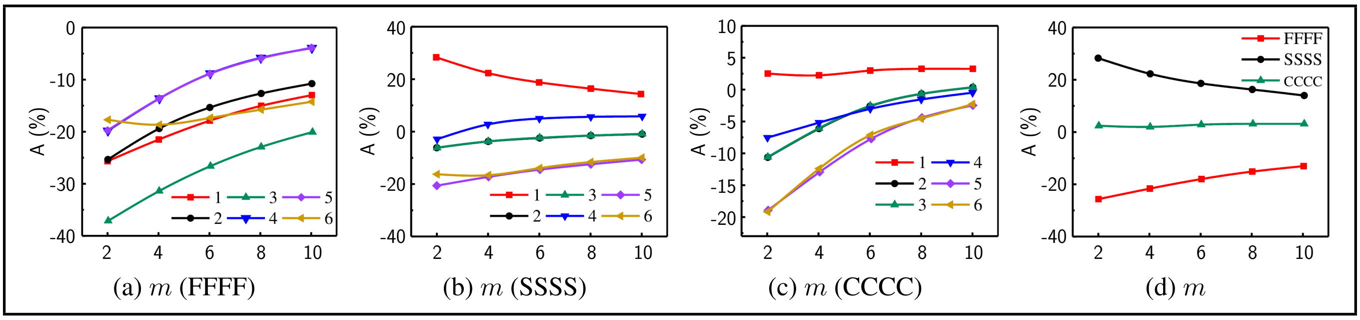

Figure 9. Percentage change of natural frequency of bidirectional nonlinear concave variable thickness plate.

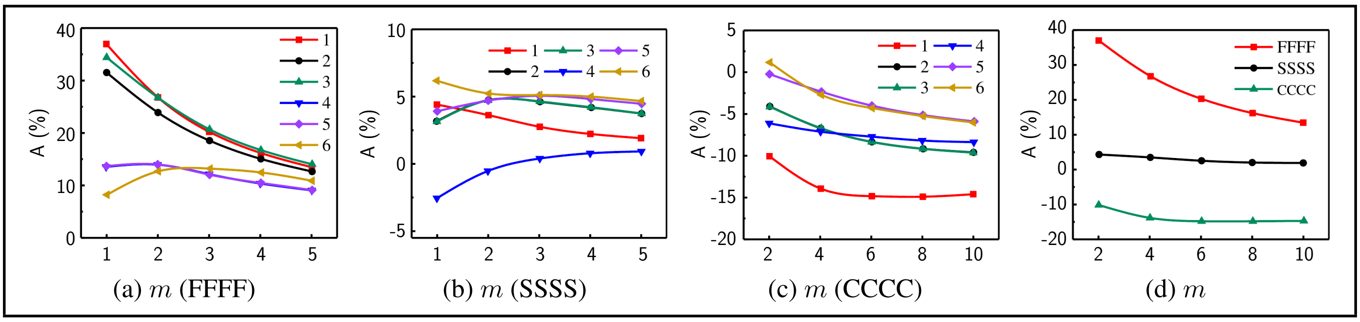

Figure 10. Percentage change of natural frequency of bidirectional nonlinear convex variable thickness plate.

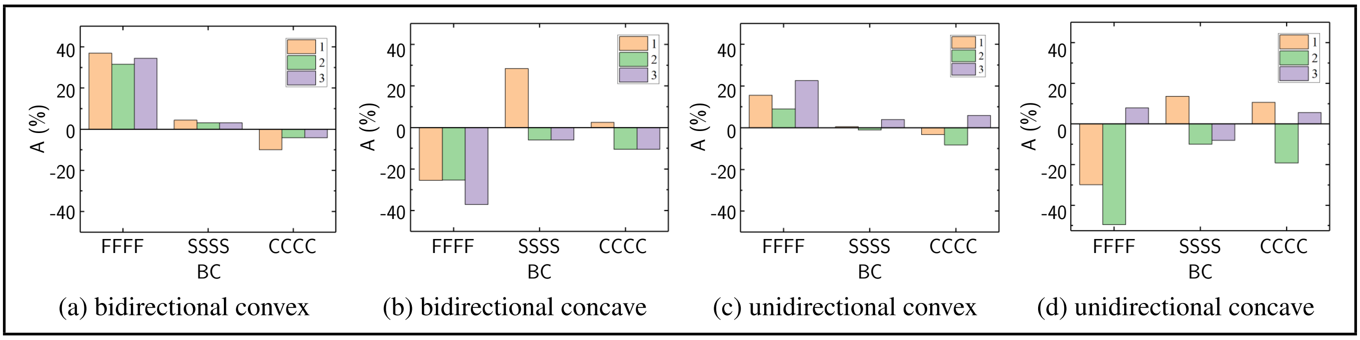

Figure 11. Percentage graph of natural frequency thin plates with different thickness.

shown in Fig. 15, the percentage change chart of the bidirectional stepped VRB natural frequency can be finally obtained.

The following conclusions can be drawn from the figures. The bidirectional stepped VRB can effectively increase the first three-order natural frequency on the free and fixed-supported boundary conditions compared to corresponding equal-thickness thin plates. However, the natural frequency does not change significantly on the simply-supported boundary. The general trend of the natural frequency percentage A is a gradually increasing trend with the increase of the middle thickness L. Besides, the first-order natural frequency under the simply supported boundary condition will decline slightly.

As shown in Fig. 14, a percentage graph of the natural frequency improvement of the bidirectional stepped variable-thickness thin plate in which the middle thickness is 2 mm. For the first-order natural frequency of the bidirectional variable-thickness thin plate, the natural frequency promoted 32.45% on the free boundary condition and 11.66% on fixed-supported boundary condition, but the natural frequency declines only 3% on the simply supported boundary condition. Based on the above figures, it can be seen that this type of thickness distribution is beneficial to the improvement of the thin plate's natural frequency.

By comparing and analyzing Fig. 12 and Fig. 14, it can be seen that the bidirectional stepped VRB's first-order natural frequency will slightly decline under three classical boundary conditions, however, the bidirectional stepped VRB's second-order and third-order natural frequency will rise substantially. Therefore, the new thickness distribution of bidirectional stepped VRB is better than the previous four conventional variable-thickness thin plates.

4.2. Optimization Design of VRB

According to the above-mentioned research, it can be seen that when bidirectional stepped VRB's other values remain unchanged, its vibration characteristics are affected by the intermediate thickness t and the step width L. When the design variables parameters t and L are selected for optimization, the final result of the optimization will obviously be another bidirectional stepped variable thickness thin plate which is not universal. Therefore, in order to make the optimization results more general, considering the structural characteristics of the new thickness distribution form is symmetry, the optimization scheme shown in Fig. 15 is adopted. The specific steps are as follows:

Firstly, the general symmetrical thickness thin plate is divided into two optimization schemes. The first scheme is the block division method, in which the thin plate is divided from the inside to the outside, and the second scheme is the ring division method, in which the thin plate is divided according to the circle.

Secondly, all the thicknesses are sorted in a ring shape from inside to outside. The thickness variables of scheme 1 from inside to outside are $t_1, t_2, \cdots, t_{10}$ and the thickness variables of scheme 2 from inside to outside are $t_1, t_2, \cdots, t_{12}$.

Since the thickness has been divided in advance, it is equivalent to what L has been determined, so only thickness needs to be determined as a design variable.

The natural frequency of the thin plate has a significant relationship with the quality, however different variable-thickness thin plates' natural frequency is only relied upon the relevant software to calculate, but cannot directly derive the relationship between the natural frequency of the variable-thickness thin plate and the quality. Therefore, we can refer to the existing calculation formula of the thin plate's natural frequency on the simple support condition. The formula is as follows:

$$\omega_{i,j} = \pi^2 \left(\frac{i^2}{a^2} + \frac{j^2}{b^2} \right) \sqrt{\frac{D}{\rho h}}; \tag{4}$$

where i and j are sorted according to the magnitude of the

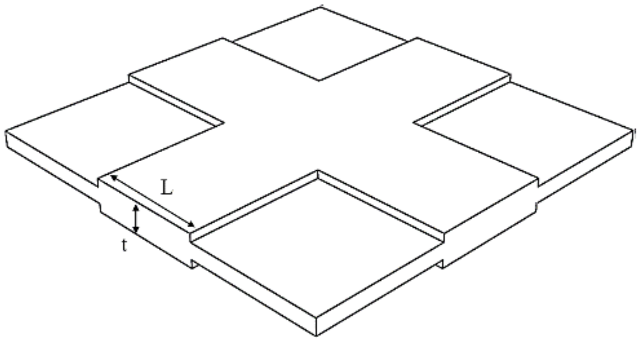

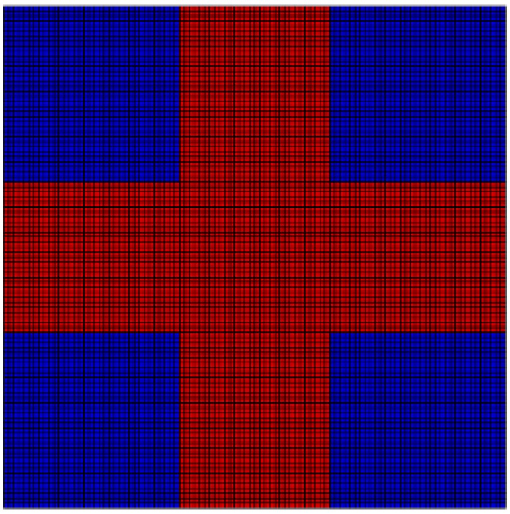

Figure 12. New thickness distribution form: unidirectional stepped VRB.

Table 4. Natural frequency of variable thickness thin plate under different qualities.

ρ (kg/m^3)	BC	f (CYCLES/TIME)					
		1	2	3	4	5	6
7800	FFFF	26.909	32.640	42.617	52.054	52.054	78.501
	SSSS	28.800	79.198	79.198	121.44	159.60	164.35
	CCCC	60.657	122.21	122.21	163.70	212.56	233.89
15600	FFFF	19.027	23.080	30.135	36.808	36.808	55.509
	SSSS	20.365	56.002	56.002	85.873	112.85	116.21
	CCCC	42.891	86.415	86.415	115.76	150.30	165.39

calculated value and correspond to the value of the first natural frequency to the nth natural frequency.

According to Eq. (4), and combined with the formulas of $\omega = 2\pi f$ and$m = \rho V$, Eq. (5) is obtained:

$$f \propto \sqrt{\frac{1}{m}}; \tag{5}$$

where f is the natural frequency, and m is the quality of the thin plate.

As shown in Table 4, in order to verify the correctness of the above-mentioned theoretical inference, bidirectional stepped variable-thickness thin plate's simulation results are used as references.

The natural frequency obtained when the density is 7800 kg/m^3 is 1.4 times that when the density is 15600 kg/m^3 on three boundary conditions according to Table 4. This proves the relationship between the natural frequency of the VRB and the mass is correct.

Based on previous analysis, the final optimization goals are determined as follows:

$$q = \frac{f^2}{m}. \tag{6}$$

In this article, the multi-island genetic algorithm is selected for optimal design and setting of the corresponding number of iterations. At the same time, the parameters need to be set from the following two aspects:

(1) Setting upper and lower limits of the variable t_i. Considering the accuracy of the simulation solution and the applicability of the thin plate theory that is obtained, the variation range of the thickness is set as $1 \leq t_i \leq 2$ mm; and,

(2) Restricting the value range of the optimization target. Meanwhile, the maximum value of q should be selected as the optimization goal, so the direction chosen is to maximize.

Following the corresponding steps to build an optimization model, the thin plate of scheme 1 has 10 design variables of thickness t_i from inside to outside, meanwhile, the side length of the square is $0.05, 0.10, \cdots, 0.5$ m in order. The thin plate of scheme 2 has 12 design variables of thickness t_i from inside to outside, and the radius of the circle is $0.03, 0.06, \cdots, 0.36$ m in turn. The parameters are as follow: $a = b = 0.5$ m, $\rho = 7800$ kg/m^3, $E = 210$ GPa, $\mu = 0.3$, and the boundary condition is fixed support. Since the number of iterations will have an important impact on the optimization results, different numbers of iterations are set to solve the corresponding optimization results.

As shown in Fig. 16 and 17, two optimization schemes have iteration times of 20, 30, 40, and 50, respectively, and the optimization times correspond to the optimization results q graphs of 2000, 3000, 4000, and 5000, respectively. The black line is the total q, and the number is equal to the corresponding optimization times, meanwhile, the red line is the increasing q.

In the optimization results, the thicknesses corresponding to the best optimization results in the four iterations are extracted in Fig. 16 and 17, and the optimized values are shown in Table. 5 and 6, respectively.

Now, $t_i/2$ is taken as the thickness from the above table, and then the thickness variation curve of the variable-thickness thin plate can be obtained as shown in Fig. 18, which is a schematic cross-section diagram of thin plate with variable thickness. Fig. 18 is the cross-sectional thickness variation curve of schemes 1 and 2 respectively, and the ordinate is the thickness value that corresponds to $t_i/2$. The abscissa represents the order i of the thickness. It can be seen with reference to Fig. 18 that scheme 1 corresponds to the change in thickness of the gray cross-section. Because scheme 2 is a circle division, when the abscissa changes in $[-10, 10]$, it is the change in cross-sectional thickness. When the abscissa changes in $[-12, 12]$, it is the change in the thickness of the oblique section, corresponding to the blue section in Fig. 18.

As is shown in Fig. 19, whether scheme 1 or scheme 2 is adopted, the optimization results have certain rules that the central thickness and both sides' thickness are large. It can be seen that when scheme 1 is used for thickness optimization design, the thickness of the thin plates' four sides approaches 2 mm, corresponding to i takes $[-10, -7]$ and $[7, 10]$. When

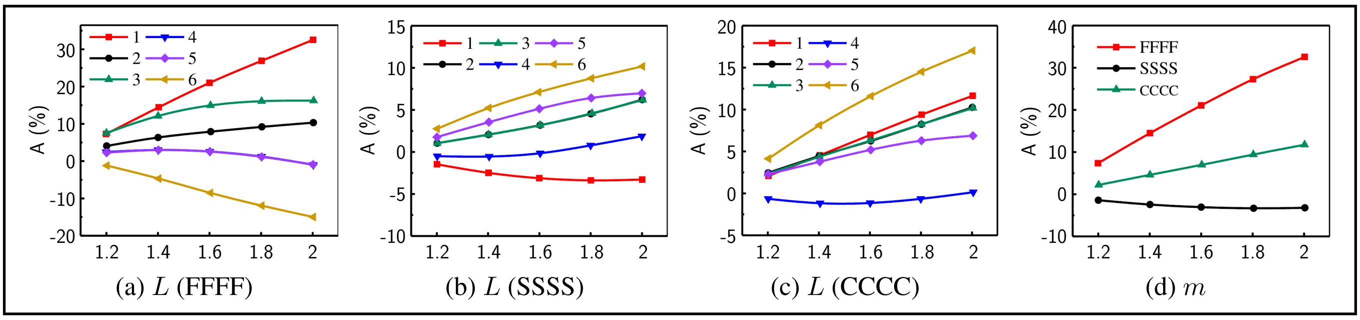

Figure 13. Change diagram of natural frequency percentage of bidirectional stepped VRB.

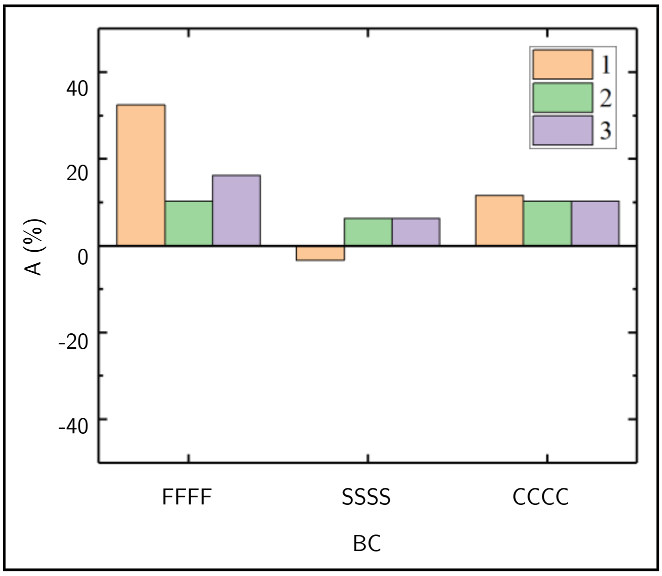

Figure 14. Percentage graph of natural frequency increase of bidirectional stepped VRB.

Table 5. q and t_i optimization of scheme 1.

N	20	30	40	50
q (Hz^2/kg)	1420.41	1432.13	1452.79	1464.45
t_1 (mm)	1.7991	1.7630	1.7366	1.2629
t_2 (mm)	1.3300	1.3419	1.3434	1.2818
t_3 (mm)	1.2833	1.2166	1.1933	1.1602
t_4 (mm)	1.0340	1.0323	1.0322	1.0303
t_5 (mm)	1.0707	1.0707	1.0543	1.0397
t_6 (mm)	1.3315	1.6685	1.6683	1.6682
t_7 (mm)	1.6897	1.7161	1.9658	1.9736
t_8 (mm)	1.9915	1.9915	1.9997	1.9997
t_9 (mm)	1.9854	1.9988	1.9971	1.9980
t_{10} (mm)	1.9972	1.9991	1.9970	1.9999

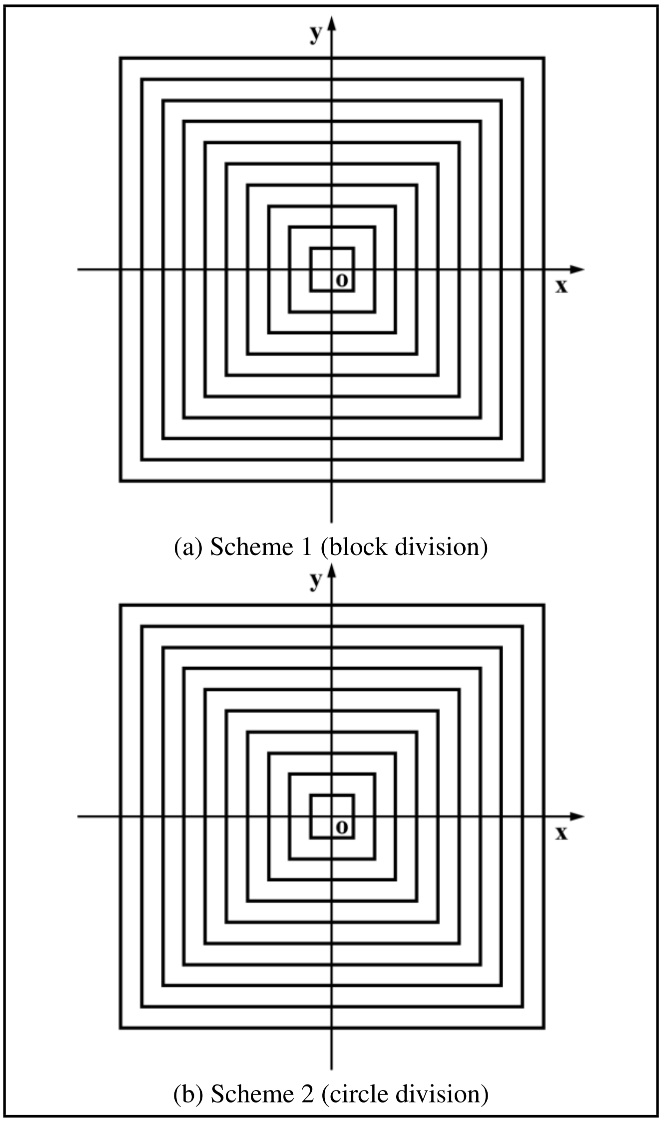

Figure 15. Schematic diagram of thickness optimization scheme.

the middle thickness of the thin plate approaches 1.3 mm, the i take $[-3, 3]$. Meanwhile, $[-7, -4]$ and $[4, 7]$ are the thickness transition zone. When scheme 2 is used for thickness optimization design, the thickness of the thin plate's four corners approaches 1mm, and the i take $[-12, -10]$ and $[10, 12]$. When the thickness values of the thin plate's four sides approach 2 mm, the i values $[-10, -6]$ and $[6, 10]$. When the middle thickness of the thin plate approaches 1.5 mm, the i value $[-3, 3]$. The $[-6, -4]$ and $[4, 6]$ are the thickness transition areas.

Combined with the comparison analysis of scheme 1 and scheme 2, it is noted that when the i value is in the $[-10, 10]$, the change rule of the corresponding cross-sectional thickness change curve is basically the same.

As shown in Fig. 20, in order to make the thickness distribution optimization results more obvious and visual, the optimized thickness t_i in Tables 5 and 6 are substituted into the thin plate model for simulation, and the corresponding thin plate distribution cloud can be solved. According to the thickness distribution optimization result cloud diagrams, as the color changes from lighter to darker, the thickness becomes thicker and the minimum value is approximately 1mm, and the maximum value is approximately 2 mm. It can be also clearly seen from Fig. 20 that both Scheme 1 and Scheme 2 gradually be-

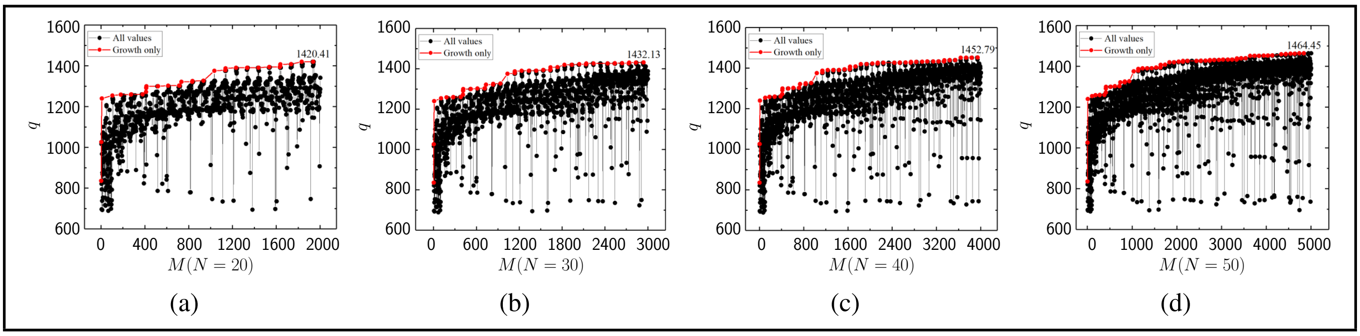

Figure 16. The optimization result of scheme 1.

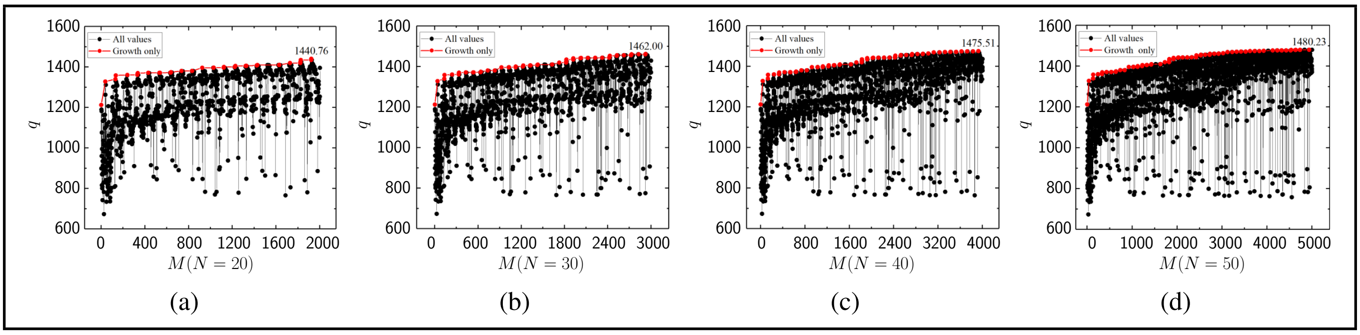

Figure 17. The optimization result of scheme 2.

Table 6. q and t_i optimization of scheme 2.

N	20	30	40	50
q (Hz^2/kg)	1440.76	1462.00	1475.51	1480.23
t_1 (mm)	1.7759	1.7749	1.7564	1.6066
t_2 (mm)	1.7013	1.6994	1.6994	1.5586
t_3 (mm)	1.7382	1.6288	1.3750	1.4413
t_4 (mm)	1.3724	1.0651	1.0651	1.0644
t_5 (mm)	1.0236	1.0243	1.0167	1.0391
t_6 (mm)	1.7068	1.6911	1.7476	1.9188
t_7 (mm)	1.9964	1.9997	1.9997	1.9440
t_8 (mm)	1.9901	1.9901	1.9943	1.9901
t_9 (mm)	1.9563	1.9807	1.9812	1.9823
t_{10} (mm)	1.9351	1.9351	1.9398	1.9742
t_{11} (mm)	1.3698	1.3387	1.3153	1.0039
t_{12} (mm)	1.6665	1.6660	1.3320	1.0447

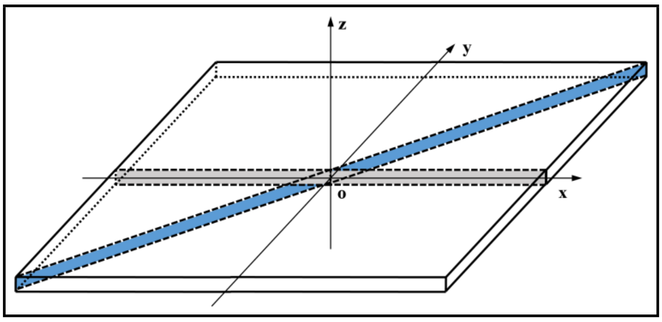

Figure 18. Schematic diagram of variable thickness thin plate.

come lighter in color near the center as the number of iterations increases. At the same time, the color of the four corners of the thin plate of scheme 2 gradually becomes lighter, which means that the thickness value gradually decreases.

Comparing the natural frequencies of thin plates with equal mass and thickness on the classical boundary conditions with the two optimized schemes when the number of iterations N is 50, Table 7 can be obtained. The first-order natural frequency of the optimized variable-thickness thin-plate in Scheme 1 increases by 7.983 Hz, and the increasing ratio is 12.79%. Meanwhile, increments of q are 313.384 Hz^2/kg, and the increasing ratio is 27.23%. In contrast, the first-order natural frequency of the variable-thickness thin-plate after optimization in Scheme 2 can increase by 8.834 Hz, and the percentage increment reaches 14.4%. The increment of q is 349.426 Hz^2/kg, and the percentage increment reaches 30.9%. At the same time, 14.4% is also higher than the lifting effect of all other variable-thickness thin plates mentioned above, which proves the effectiveness of the optimization results. Finally, it is seen that the optimization result of Scheme 2 is better than Scheme 1 by comparing the increased percentage values.

Table 7. Optimization results of natural frequencies of the two schemes.

Scheme	Before and after optimization	f (Hz) CCCC		FFFF	q (Hz^2/kg)	mass (kg)
Scheme 1	Before	62.395	34.193	23.332	1151.066	3.3822
	After	70.378	34.067	21.741	1464.450	
	Boost value	7.983	-0.126	-1.591	313.384	
	Lift percentage	12.79%	—	—	27.23%	
Scheme 2	Before	61.297	33.593	22.922	1130.806	3.323
	After	70.131	33.218	23.543	1480.232	
	Boost value	8.834	-0.375	0.621	349.426	
	Lift percentage	14.4%	—	—	30.9%	

4.3. Finite Element Segmentation Method Scheme

As shown in Fig. 21, although both optimization schemes can improve the natural frequency based on equal thickness thin plates, there is still room to improve the final optimization results of schemes 1 and 2. Compared scheme 1 with 2, it is found that the thickness of the four corners of the sheet should be close to 1 mm. However, due to the division of the squares,

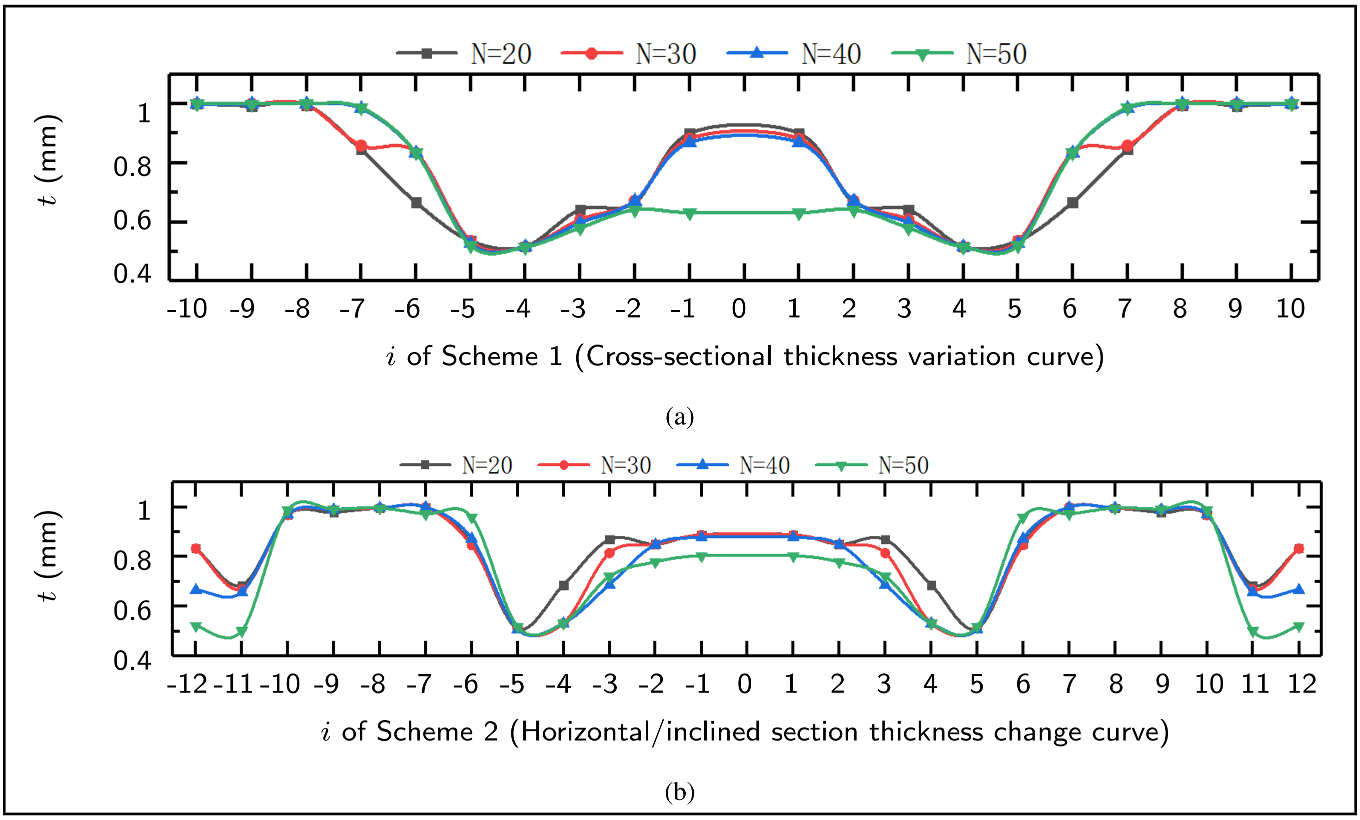

Figure 19. Curve of section thickness variation.

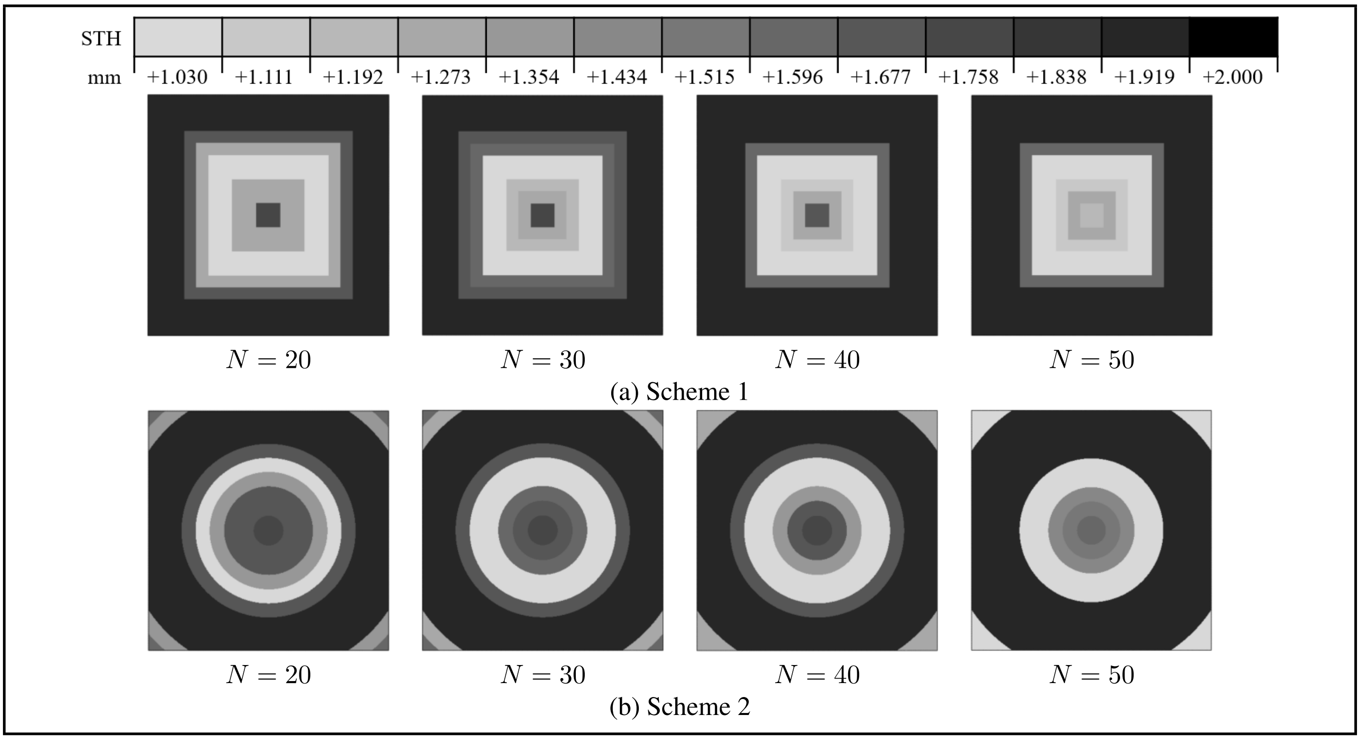

Figure 20. Cloud chart of optimization results of variable thickness thin plate.

the thickness of the four corners in Scheme 1 is equal to 2 mm.

The finite element segmentation method (FESM) is used to optimize the area of the thin plate. Therefore, the thin plate is divided into small unit shapes. In order to make the simulation results close to the ideal situation, the thin plate is refined as much as possible. As shown in Fig. 21, the thin plate is divided into 10×10 small units classified according to symmetry, and they are sorted from inside to outside in order. For example, there are 4 thickness units with the number 1 with equal thickness, and number 2 has 8 thickness units with equal thickness. By analogy, the improvement scheme in Fig. 21 has a total of 15 thicknesses.

As shown in Fig. 22, different iteration times are set to solve the corresponding optimization results. With the increase of

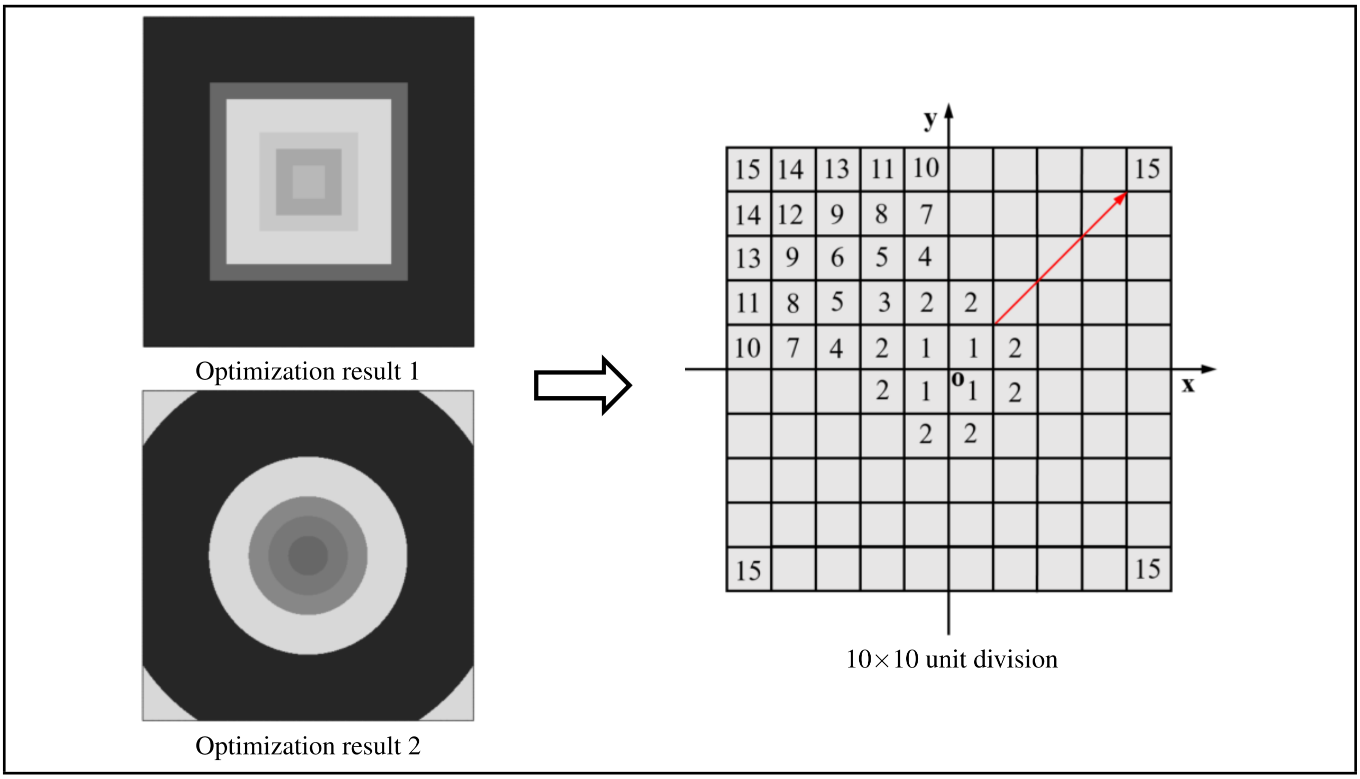

Figure 21. Improved optimization program.

Table 8. q and t_i optimization of improved scheme.

N	20	30	40	50
q (Hz^2/kg)	1456.84	1481.59	1498.03	1514.30
t_1 (mm)	1.1023	1.2273	1.4002	1.2411
t_2 (mm)	1.2784	1.2784	1.0343	1.0948
t_3 (mm)	1.0951	1.0963	1.0137	1.0963
t_4 (mm)	1.0106	1.0106	1.0235	1.0184
t_5 (mm)	1.4067	1.1567	1.5198	1.0787
t_6 (mm)	1.9037	1.9935	1.8614	1.9989
t_7 (mm)	1.9698	1.9755	1.8046	1.9746
t_8 (mm)	1.8654	1.8846	1.8777	1.8971
t_9 (mm)	1.926	1.926	1.9301	1.9334
t_{10} (mm)	1.9773	1.9772	1.9675	1.9839
t_{11} (mm)	1.9914	1.9914	1.9934	1.9913
t_{12} (mm)	1.0363	1.0887	1.0435	1.0575
t_{13} (mm)	1.839	1.839	1.9287	1.9647
t_{14} (mm)	1.2048	1.0459	1.0371	1.0479
t_{15} (mm)	1.1101	1.0774	1.053	1.0698

the number of iterations, the change of q value gradually decreases, and compared to the Scheme 1 and 2, the optimization target q under each iteration number is larger. It can be seen that the improved optimization program is better than Scheme 1 and 2 which proves the effectiveness and correctness of this improvement scheme.

The corresponding thickness after the optimization under the four iteration times is extracted and shown in Table. 8, which corresponds to the optimization results of the thickness and q under the number of iterations $N = 20$, 30, 40 and 50, respectively.

Figure 23 is drawn by the above thickness values according to the number of iterations. It can be seen that the thickness change curves under the four iterations are basically the same. Since the FESM is completely different from the previous two schemes, Fig. 23 is not a cross-section in a practical sense.

The corresponding cloud map of the thickness distribution is solved as shown in Fig. 24. It can be clearly seen that as the number of iterations increases, the color near the center of the thin plate gradually becomes lighter, which means that thickness value decreases. At the same time, the color at the four corners of the thin plate also gradually changes shallow, which means that the thickness gradually decreases.

Compared with the previous two schemes, the FESM scheme's optimization target q has been greatly improved, which can further study the feasibility of the FESM scheme. As shown in Fig. 25, the unit is divided more finely and the thin plate is divided into 20×20 small units. At this time, there are 55 kinds of thickness.

Since the thickness parameter is increased from 15 to 55, the number of iterations is set to 150 times with considering the optimization calculation time. As shown in Fig. 26, it is an optimization result graph with 150 iterations after 15,000 optimizations. It can be seen from the figure that the division is more detailed, but it also leads to a case where there are too many thickness parameters. Even if the number of iterations is expanded to 3 times the original, the final q value is 1501.62 Hz^2/kg, which cannot reach the optimization result q for 50 iterations of 10×10 unit division.

As shown in Fig. 27, the corresponding thickness distribution cloud is solved. The color spectrum on the left uses rainbow colors, and the color spectrum on the right uses black and white. It can be seen that its distribution form is basically consistent with the previous 10×10 unit division. When taking the calculation time and optimization results into account, it is not difficult to find that it is better to use 10×10 unit division.

Similarly, the natural frequency of the thin plates of equal mass and equal thickness by the method of FESM is obtained by simulation, and the specific values are shown in Table. 9. It can be found that when the boundary condition is fixed support, the optimized first-order natural frequency of the variable-thickness thin plate can be effectively increased by

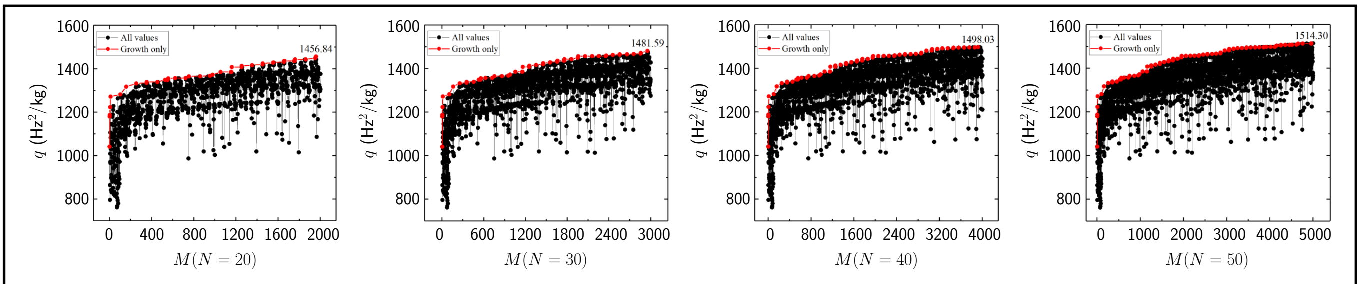

Figure 22. Optimization result diagram of the improved scheme.

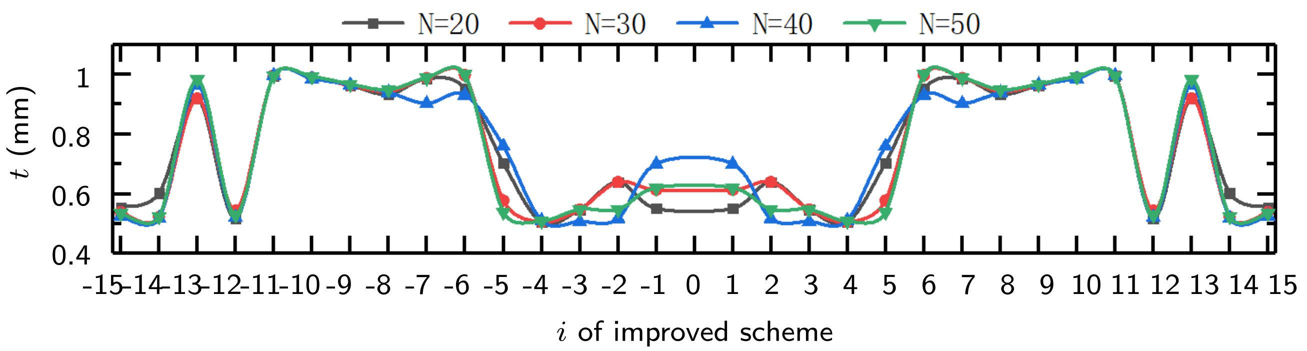

Figure 23. Thickness variation curve of unit division method.

Table 9. The optimized result of natural frequency after improving the schemes 1and 2.

f (Hz)	CCCC	SSSS	FFFF	q (Hz^2/kg)	mass (kg)
Before	67.376	28.634	22.276	1514.30	2.998
After	55.305	30.312	20.683	1020.30	
Boost value	12.071	-1.678	1.593	493.99	
Lift percentage	21.8%	—	—	48.4%	

12.071 Hz, and the percentage increase reaches 21.8%. What's more, the value of q increases by 493.99 Hz^2/kg, and the percentage increase reaches 48.4%. However, the difference between the first-order natural frequency of the other two boundary conditions is small, the percentage of 21.8% is also higher than the lifting effect of the other two optimization schemes in Section 4.2 which proves the effectiveness of the improved scheme.

As shown in Fig. 28 which plots the optimized values of the above-mentioned scheme 1 and scheme 2, and the improved scheme into a curve. It can be seen from the above figure that the value of the first-order natural frequency and the optimization target q increases.

5. CONCLUSION REMARKS

In this paper, the vibration characteristics of four kinds of thin plates with variable thickness were analyzed and compared with those of uniform thin plates of equal mass. Then, based on the variation law of the vibration characteristics of the four kinds of variable thickness thin plates, a new type of stepped variable thickness thin plate was proposed. Finally, inspired by the step-by-step idea, the square and circular division methods were used to improve the natural frequency of the variable-thickness thin plate, and the optimal design is carried out. Some remarkable conclusions could be obtained as follows:

(1) The vibration characteristics of four kinds of thin plates with different variable thickness forms were analyzed to study the variation of vibration characteristics with thickness under different boundary conditions and compared with the corresponding equal mass thin plates of uniform thickness. The result showed that unidirectional linear, bidirectional linear, unidirectional nonlinear convex and Bidirectional nonlinear convex were not beneficial to the enhancement of natural frequency, while unidirectional nonlinear concave and Bidirectional nonlinear concave was beneficial to the enhancement of the natural frequency.

(2) A novel bidirectional step-variable-thickness thin plate was proposed, which satisfies the thickness distribution requirements on both the central and four edges. The results show that the bi-directional stepped variable thickness thin plate can effectively improve its first 3 orders of natural frequency under free and solid support boundary conditions relative to its corresponding equal mass and equal thickness thin plate. With the increase of the middle thickness of the step L, the overall trend of the percentage of the natural frequency A showed a gradually increasing trend.

(3) Inspired by the results, a new bidirectional stepped VRB was proposed to improve the natural frequency of variable-thickness thin plate. The square division method and circle division method were employed to further improve the natural frequency of variable-thickness thin plate. The results showed that all indicators have been improved, among which the first-order natural frequency has increased by 12.071 Hz, accounting for 21.8%, and the optimization target q has increased by 493.99 Hz^2/kg, accounting for 48.4%.

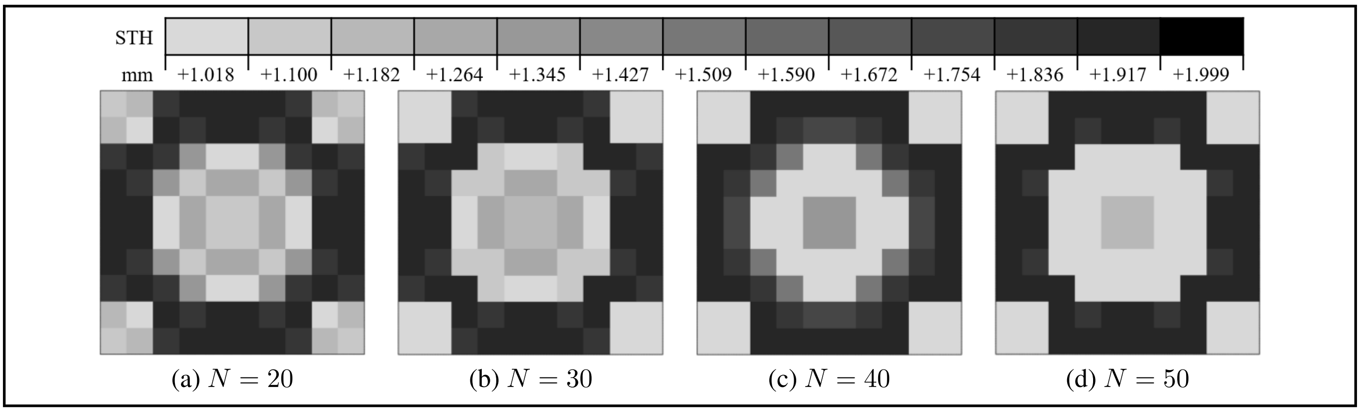

Figure 24. Optimal results of thickness distribution after improved scheme.

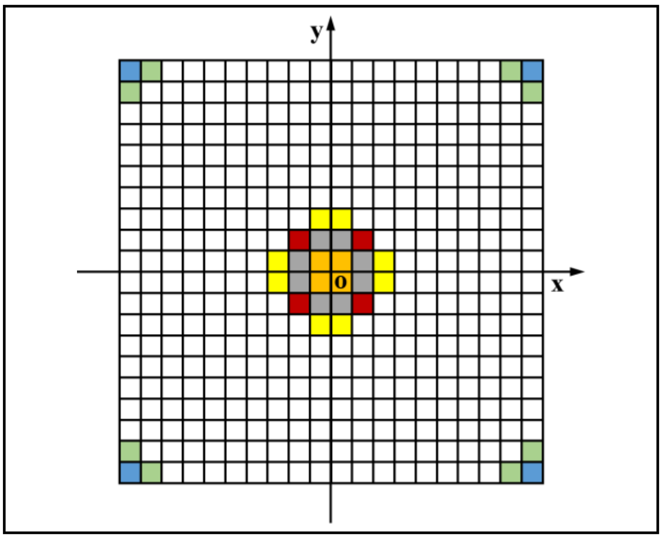

Figure 25. 20×20 unit division.

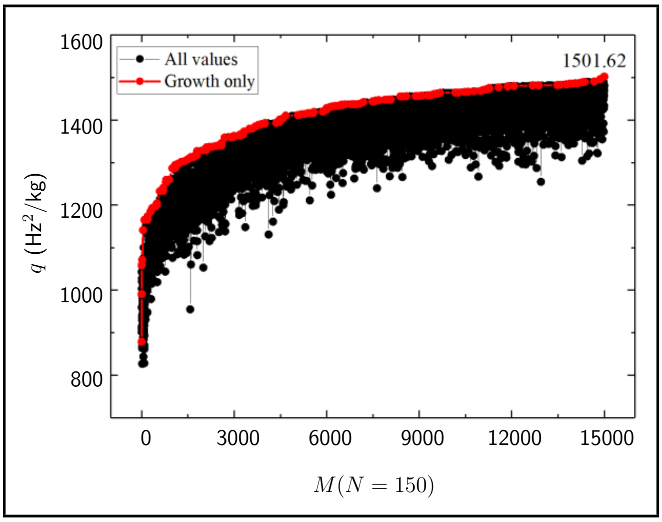

Figure 26. 20×20 unit division optimization results.

ACKNOWLEDGEMENTS

The support of this work by the National Natural Science Foundation of China (51975438, U1564202) is greatly appreciated. The work was also supported by the 111 Project (B17034).

REFERENCES

[1] Ohga, M., Shigematsu, T., Bending analysis of plates with variable thickness by boundary element-transfer matrix method, *Comput. Struct.*, **28**, 635–641, (1988). https://doi.org/10.1016/0045-7949(88)90008-9

[2] Fertis, D.G., Lee, C.T., Elastic and inelastic analysis of variable thickness plates by using equivalent systems, *Int. J. Mech. Struct. Mach.*, **21**(2), 201–211, (1993). https://doi.org/10.1080/08905459308905187

[3] Chaves, E.W.V., Fernandes, G.R., Venturini, W.S., Plate bending boundary element formulation considering variable thickness, *Eng. Anal. Bound. Elem.*, 23(5-6), 405–418, (1999). https://doi.org/10.1016/s0955-7997(98)00097-6

[4] Zenkour, A.M., Elastic behaviour of an orthotropic beam/one-dimensional plate of uniform and variable thickness, *J. Eng. Math.*, **44**(4), 331–344, (2002). https://doi.org/10.1023/A:1021255410184

[5] Hadji, L., Avcar, M., Zouatnia, N., Natural frequency analysis of imperfect FG sandwich plates resting on Winkler-Pasternak foundation. *In Polymer and Mediterranean Fiber International Conference*, Bejaia, Algeria, (1998). https://doi.org/10.1016/j.matpr.2021.12.485

[6] Civalek, O., Avcar, M., Free vibration and buckling analyses of CNT reinforced laminated non-rectangular plates by discrete singular convolution method, *Eng Comput-Germany.*, **38**(Suppl 1), 489–521, (2022). https://doi.org/10.1007/s00366-020-01168-8

[7] Meksi, R., Benyoucef, S., Mahmoudi, A., Tounsi, A., Bedia, E.A., Mahmoud, S.R., An analytical solution for bending, buckling and vibration responses of FGM sandwich plates, *J Sandw Struct Mater.*, **21**(2), 727–757, (2019). https://doi.org/10.1177/1099636217698443

[8] Hadji, L., Avcar, M., Civalek, O., An analytical solution for the free vibration of FG nanoplates, *J Braz Soc Mech Sci.*, **43**(9), (2021). https://doi.org/10.1007/s40430-021-03134-x

[9] Daikh, A.A., Zenkour A.M., Free vibration and buckling of porous power-law and sigmoid functionally graded

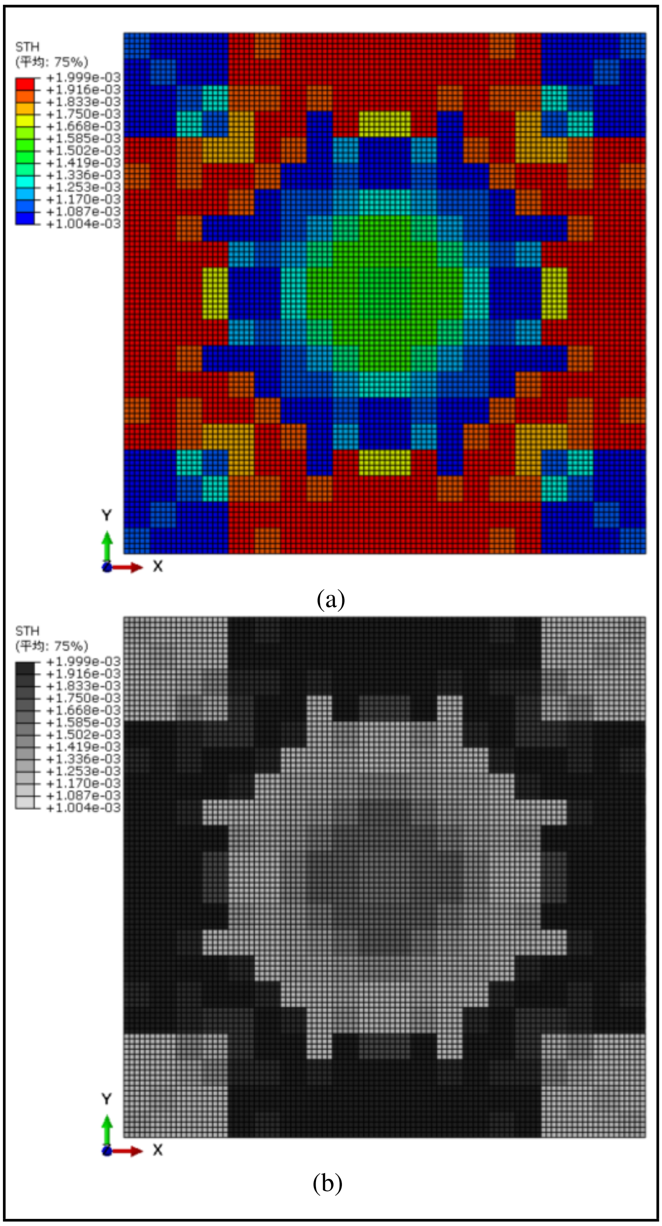

Figure 27. 20×20 unit divided thickness distribution cloud.

sandwich plates using a simple higher-order shear deformation theory, *Mater Res Experss.*, **6**(11), (2019). https://doi.org/10.1088/2053-1591/ab48a9

10 Appl, F., Byers, N., Fundamental frequency of simply supported rectangular plates with linearly varying thickness, *J. Appl. Mech*, **32**(1), 163–168, (1965). https://doi.org/10.1115/1.3625713

11 Ashton, J. E., Free Vibration of Linearly Tapered Clamped Plates, *J Eng Mech*, **95**(2), 497–500, (1969). https://doi.org/10.1061/jmcea3.0002942

12 Aksu, G., Ali, R., Free vibration analysis of stiffened plates using finite difference method, *J Sound Vib*, **48**(1), 15–25, (1976). https://doi.org/10.1016/0022-460X(76)90367-9

13 Civalek, Ö., Harmonic differential quadrature-finite differences coupled approaches for geometrically nonlinear static and dynamic analysis of rectangular plates on elastic foundation, *J Sound Vib*, **294**(4–5), 966–980, (2006). https://doi.org/10.1016/j.jsv.2005.12.041

14 Macneal, R., The solution of elastic plate problems by electrical analogies, *J Appl Mech-T ASME*, **18**(1), 59–67, (1951). https://doi.org/10.1115/1.4010221

15 Nash, W., Several approximate analyses of the bending of a rectangular cantilever plate by uniform normal pressure, *J Appl Mech-T ASME.*, **19**(1), 33–36, (1952). https://doi.org/10.1115/1.4010403

16 Fo-Van, C., Bending of uniformly cantilever rectangular plates, *J. Appl. Math. Mech.*, **1**(3), 371–383, (1980). https://doi.org/10.1007/BF01874559

17 Silva, A. R., Silveira, R. A., Gonçalves, P. B., Numerical methods for analysis of plates on tensionless elastic foundations, *Int. J. Solids Struct.*, **38**(10–13): 2083–2100, (2001). https://doi.org/10.1016/S0020-7683(00)00154-2

18 Nguyen-Thanh, N., Rabczuk, T., Nguyen-Xuan, H., Bordas, S.P.A., A smoothed finite element method for shell analysis, *Compute Method Appl. M.*, **198**(2), 165–177, (2008). https://doi.org/10.1016/j.cma.2008.05.029

19 Mlzusawa, T., Vibration of rectangular Mindlin plates with tapered thickness by the spline strip method, *Comput. Struct.*, **46**(3), 451–463, (1993). https://doi.org/10.1016/0045-7949(93)90215-Y

20 Bert, C., Malik, M., Free vibration analysis of tapered rectangular plates by differential quadrature method: a semi-analytical approach, *J Sound Vib.*, **190**(1), 41-6, (1996). https://doi.org/10.1006/jsvi.1996.0046

21 Donning, B. M., Liu, W. K., Meshless methods for shear-deformable beams and plates, *Compute Method Appl M.*, **152**(1–2), 47–71, (1998). https://doi.org/10.1016/S0045-7825(97)00181-3

22 Sakiyama, T., Huang, M., Free vibration analysis of rectangular plates with variable thickness, *J Sound Vib.*, **216**(3), 379–397, (1998). https://doi.org/10.1006/jsvi.1998.1732

23 Malekzadeh, P., Shahpari, S., Free vibration analysis of variable thickness thin and moderately thick plates with elastically restrained edges by DQM, *Thin Wall Struct.*, **43**(7), 1037–1050, (2005). https://doi.org/10.1016/j.tws.2004.11.008

24 Singh, B., Saxena, V., Transverse vibration of a rectangular plate with bidirectional thickness variation, *J Sound Vib.*, **198**(1), 51–65, (1996). https://doi.org/10.1006/jsvi.1996.0556

25 Ashour, A., Vibration of variable thickness plates with edges elastically restrained against translation and rotation, *Thin Wall Struct.*, **42**(1), 1–24, (2004). https://doi.org/10.1016/S0263-8231(03)00127-7

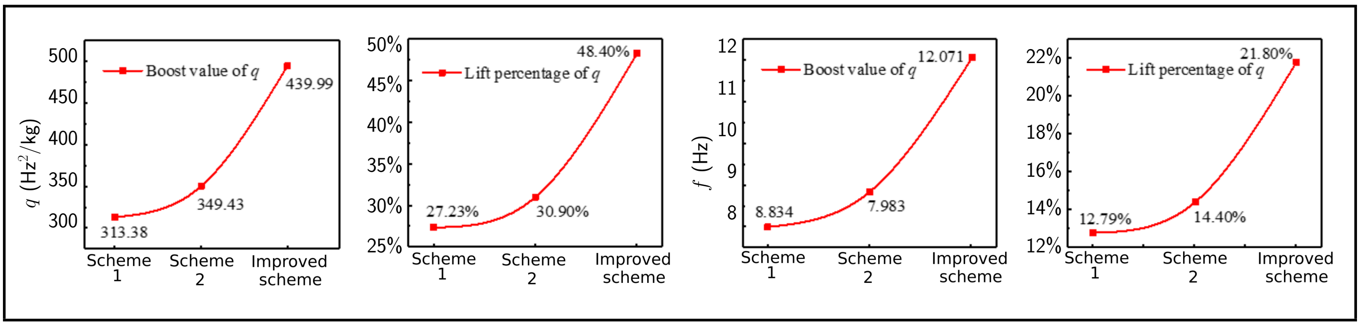

Figure 28. Comparison of optimization results of different schemes.

[26] Li, W.L., Vibration analysis of rectangular plates with general elastic boundary supports, *J Sound Vib.*, **273**(3), 619–635, (2004). https://doi.org/10.1016/S0022-460X(03)00562-5

[27] Li, W.L., Zhang, X.F., Du, J.T., Liu, Z.G., An exact series solution for the transverse vibration of rectangular plates with general elastic boundary supports, *J Sound Vib.*, **321**(1-2), 254–269, (2009). https://doi.org/10.1016/j.jsv.2008.09.035

[28] Ye, T.G., Jin, G.Y., Su, Z., Chen, Y.H., A modified Fourier solution for vibration analysis of moderately thick laminated plates with general boundary restraints and internal line supports, *Int. J. Mech. Sci.*, **80**, 29–46, (2014). https://doi.org/10.1016/j.ijmecsci.2014.01.001

[29] Yuan, J.H., Chen, W.Q., Exact solutions for axisymmetric flexural free vibrations of inhomogeneouscircular Mindlin plates with variable thickness, *Appl. Math. Mech.-Engl. Ed.*, **38**, 505–526, (2017). https://doi.org/10.1007/s10483-017-2187-6

[30] Xu, Y.P., Zhou, D., Three-dimensional elasticity solution for simply supported rectangularplates with variable thickness, *J. Strain Anal. Eng.*, *De*, **43**(3), 165–176, (2008). https://doi.org/10.1243/03093247JSA353

[31] Xu, Y. P., Zhou, D., Three-dimensional elasticity solution of functionally graded rectangularplates with variable thickness, *Compos. Struct.*, **91**(1), 56–65, (2009). https://doi.org/10.1016/j.compstruct.2009.04.031

[32] Vivio, F., Vullo, V., Closed form solutions of axisymmetric bending of circular plates having non-linear variable thickness, *Int. J. Mech. Sci.*, **52**(9), 1234–1252, (2010). https://doi.org/10.1016/j.ijmecsci.2010.05.011

[33] Dozio, L., Carrera, E., A variable kinematic Ritz formulation for vibration study of quadrilateral plates with arbitrary thickness. *J Sound Vib.*, **330**(18–19), 4611–4632, (2011). https://doi.org/10.1016/j.jsv.2011.04.022

[34] Semnani, S. J., Attarnejad, R., Firouzjaei, R. K., Free vibration analysis of variable thickness thin plates by two-dimensional differential transform method. *Acta Mech.*, **224**, 1643–1658, (2013). https://doi.org/10.1007/s00707-013-0833-2

[35] Thai Chien, H., Ferreira, A. J. M., Bordas, S. P. A., Rabczuk, T., Nguyen-Xuan, H., Isogeometric analysis of laminated composite and sandwich plates using a new inverse trigonometric shear deformation theory, *Compos Struct.*, **104**, 196–214, (2013). https://doi.org/10.1016/j.compstruct.2013.04.002

[36] Mashat, D. S., Zenkour A. M., Hygrothermal bending analysis of a sector-shaped annularplate with variable radial thickness, *Compos. Struct.*, **113**, 446–458, (2014). https://doi.org/10.1016/j.compstruct.2014.03.044

[37] Zenkour, A. M., Bending of thin rectangular plates with variable-thickness in a hygrothermal environment, *Thin Wall Struct.*, **123**, 333–340, (2018). https://doi.org/10.1016/j.tws.2017.11.038

[38] Chou, F. S., Zenkour, A. M., Optimization of linear segmented circular Mindlin plates for maximum fundamental frequency, *Struct Optimization.*, **11**(2), 128–133, (1996). https://doi.org/10.1007/BF01376856

[39] Belblidia, F., Hinton E., Fully integrated design optimization of plate structures, *Finite Elem Anal Des.*, **38**(3), 227–244, (2002). https://doi.org/10.1016/S0168-874X(01)00060-9

[40] Kim, D. K., Thermal optimization of plate-fin heat sinks with fins of variable thickness under natural convection. *Int. J. Heat Mass Transfer.*, **55**(4), 752–761, (2012). https://doi.org/10.1016/j.ijheatmasstransfer.2011.10.034

[41] Lee, D., Shin, S., Optimizing structural topology patterns usingregularization of heaviside function. *Struct Eng Mech.*, **55**, 1157–1176, (2015). https://doi.org/10.12989/sem.2015.55.6.1157

[42] Banh, T. T., Lee, D., Multi-material topology optimization design for continuum structures with crack patterns. *Compos Struct.*, **186**, 193–209, (2018). https://doi.org/10.1016/j.compstruct.2017.11.088

[43] Banh, T. T., Lee, D., Topology optimization of multi-directional variable thickness thin plate with multiple materials. *Struct Multidiscip O.*, **59**(5), 1503–1520, (2019). https://doi.org/10.1007/s00158-018-2143-8